To appear in:

Journal of Theoretical and Applied Physics

Online ISSN: 2251-7235 Print ISSN: 2251-7227

Received: 24 February 2026
Revised: 06 April 2026
Accepted: 26 April 2026

DOI: https://doi.org/10.57647/jtap.2026.2005.05

Research Article

Inelastic Electron-Scattering Form Factors in ^{19}F: A Shell-Model Investigation of Positive and Negative Parities

Ali A. Mohsin*, Fouad A. Majeed

Department of Physics, College of Education for Pure Sciences, University of Babylon, Babylon, Iraq

***Corresponding Author:** pure985.ali.abad@student.uobabylon.edu.iq

ORCID: https://orcid.org/0009-0002-8639-1294

Abstract

We present a comprehensive shell-model study of ^{19}F focusing on inelastic longitudinal and transverse electron-scattering form factors, excitation energies, and electromagnetic transition strengths for both positive- and negative-parity states. The calculations are carried out within the zbm model space using the ZBMI effective interaction, providing a consistent and unified description of nuclear structure and configuration mixing for both parities. The novelty of this work lies in performing a controlled and systematic comparison of different single-particle radial wave functions-Skyrme (Sk29), Woods-Saxon (WS3), and harmonic oscillator (HT)-within the same shell-model framework. This approach allows isolating the role of radial structure in determining electromagnetic observables without introducing additional model-dependent uncertainties. The electromagnetic matrix elements are calculated using radial wave functions generated from different mean-field potentials, enabling a detailed investigation of their impact on the calculated observables. In particular, the sensitivity of form factors to variations in radial behavior is examined over a wide range of momentum transfer. The calculated excitation energies and transition strengths show reasonable agreement with experimental data, confirming the reliability of the adopted interaction and model space. The results reveal a pronounced dependence of inelastic electron-scattering

form factors on the choice of radial potential, especially at intermediate and high momentum transfer, where differences in radial tails and nodal structure significantly affect both the magnitude and diffraction patterns. The Skyrme-based radial wave functions provide a more consistent overall description compared to Woods-Saxon and harmonic oscillator potentials. All calculations are performed using the NuShellX@MSU code within a unified computational framework to ensure consistency, reproducibility, and a direct comparison between different potentials and parities.

Keywords: Shell model; ^{19}F; Skyrme interaction; sd–shell nuclei; Electron-Scattering Form Factors.

1.Introduction

Electron-nucleus scattering is a well-established and powerful tool for probing nuclear structure, both in the ground state and during transitions to excited states, owing to the weak and well-characterized electromagnetic interaction governed by quantum electrodynamics. This characteristic enables nuclear properties to be extracted with minimal ambiguity. The sd-shell region is particularly suitable for such investigations, as it contains nuclei that can be successfully described within the shell model while also exhibiting collective and deformed features. The nucleus ^{19}F represents a light odd-A nuclear system complex enough to exhibit many-body correlations, making it an ideal candidate for detailed structural studies.

Early electron scattering investigations on ^{19}F focused on low- lying positive-parity states, as first reported in the work of Hallowell and co-workers [1]. Subsequently, Qyamada and collaborators extracted longitudinal and transverse form factors associated with electric multipole excitations of low-lying states, revealing limitations of the adopted nuclear models at higher momentum transfer [2]. Further measurements by Brown and colleagues extended these investigations by determining longitudinal and transverse form factors for the ground-state rotational band over a broad range of momentum transfer, demonstrating good agreement with theoretical predictions at low q and noticeable deviations at higher q [3]. From a theoretical perspective, several studies based on the variation-after-projection Hartree-Fock (VPHF) framework have shown that longitudinal form factors are

satisfactorily described at low momentum transfer. Nevertheless, noticeable deviations remain at higher q values, largely attributed to the restricted model space adopted in those calculations [4]. In a related approach, Sakuda's cluster-model analysis emphasized the importance of cluster degrees of freedom in reproducing magnetic and transverse form factors. While a generally good agreement with experimental data was achieved for the ground-state rotational band, certain limitations persisted for transitions involving higher multipolarities [5].

More recently, microscopic no-core shell-model calculations incorporating high-energy configurations were carried out by Radhi and collaborators, demonstrating that such configurations are crucial for improving the description of longitudinal form factors, while transverse form factors exhibit a weaker sensitivity and retain noticeable discrepancies [6]. Obaid and Majeed investigated sd-shell nuclei using large-basis shell-model calculations and showed that core-polarization contributions from configurations beyond the sd-shell are essential for reproducing longitudinal form factors and electric transition strengths, particularly $B(C2)\ and\ B(C4)$, without introducing adjustable parameters [7]. In particular, they showed that treating core polarization via effective proton and neutron charges is essential to reproduce longitudinal inelastic form factors, whereas transverse form factors remain governed primarily by the underlying shell-model wave functions [8]. Obaid, Majeed, and collaborators extended these studies to nuclei in the p-and sd-shell regions by adopting an enlarged $spsdpf$ model space, confirming that truncated (0+2) ħω configurations and effective charges significantly improve the level of agreement between calculated and experimental longitudinal form factors for sd-shell nuclei such as ^{28}Si [9]. Further sd-shell benchmarks reported that longitudinal C0, C2, and C4 form factors for ^{24}Mg, ^{28}Si, and ^{32}S can be reliably reproduced within $USDA$ when core polarization is included through effective charges [10]. Related p-and sd-shell calculations for ^{7}Li, ^{9}Be, and ^{24}Mg likewise indicated improved overall consistency with experimental systematics once core polarization is incorporated via effective proton and neutron charges [11]. Previous studies have shown that the choice of single-particle potentials significantly influences electron-scattering form factors and nuclear structure properties. In particular, calculations using different radial potentials such as HO, WS, and Skyrme demonstrate varying levels of agreement with experimental data,

highlighting the sensitivity of electromagnetic observables to radial wave functions [12].

Despite the extensive literature on ^{19}F, most previous studies have employed a fixed choice of radial wave functions, which limits the ability to assess the sensitivity of calculated observables to the underlying nuclear mean-field potential. In particular, longitudinal and transverse form factors are strongly dependent on the radial behavior of single-particle wave functions, especially at intermediate and high momentum transfer. Motivated by these considerations, a systematic comparison of different radial wave functions within a unified shell-model framework is required to clarify their role in shaping electromagnetic observables. In the present work, the Sk29 interaction is adopted as a representative Skyrme parameterization with established reliability in describing medium-mass nuclei, while differing from other parameterizations such as Sk28 and Sk35 used in previous studies, which are optimized for different nuclear regions and observables. The Woods-Saxon (WS3) potential provides a phenomenological description with realistic surface properties, whereas the harmonic oscillator (HT) basis is included as a reference model. The objective of this work is to quantify how the choice of radial wave functions affects inelastic electron-scattering form factors for both positive- and negative-parity states in ^{19}F within a consistent theoretical framework that allows a direct assessment of radial effects on both longitudinal and transverse responses.

Beyond electromagnetic probes, non-truncated sd-shell calculations using $USDA/USDB$ were also shown to provide an overall consistent description of Gamow-Teller strength distributions in ^{23}Na→^{23}Mg and ^{23}Na→^{23}Ne when standard quenching is applied, supporting the robustness of sd-shell effective interactions for spin-isospin observables [13]. In addition, Talib and Majeed investigated elastic and inelastic electron-scattering form factors for selected pf-shell nuclei using NuShellX@MSU, employing Skyrme-type interactions (Sk28, Sk35, Sk43) alongside GXPF1A and JUN45, and incorporating core-polarization effects via the Tassie model with effective charges [14]. In this work, we provide a systematic account of the inelastic longitudinal and transverse electron-scattering form factors for low-lying states of both parities in ^{19}F within the shell-model framework. A central aspect of the present analysis is the controlled use of different single-particle radial wave functions, generated using the SK29 Skyrme parametrization, the WS3 Woods-Saxon potential, and the harmonic-oscillator (HO) basis, to assess how the

underlying radial structure influences the diffraction pattern and the momentum-transfer dependence of the form factors. In parallel with these ^{19}F-focused studies, quantum Monte Carlo benchmarks emphasize the significant role of two-body electromagnetic currents in transverse responses, especially at higher momentum transfer [15]. Moreover, IMSRG ab initio studies highlight the importance of controlled model-space convergence [16].

Notwithstanding these comprehensive experimental and theoretical endeavors, a cohesive characterization of inelastic longitudinal and transverse electron scattering form factors for both positive-and negative-parity states in ^{19}F, integrating shell-model wave functions with Hartree-Fock single-particle states, has not yet been reported. This study aims to provide a systematic and consistent description of longitudinal and transverse inelastic electron- scattering form factors for low-lying states of both positive and negative parity in ^{19}F, using shell-model wave functions combined with Hartree-Fock single-particle states. The shell-model computations are carried out using the NuShellX@MSU code [17]. The calculated form factors, excitation energies, and transition strengths are then systematically compared with the available experimental measurements over a wide momentum-transfer range to assess the quality of the adopted wave functions and transition operators, and to identify the q-regions and multipolarities where additional correlations and effective-operator corrections become significant.

2. Theory and Methodology

This section outlines the theoretical framework and computational approach adopted in this study. It establishes the fundamental principles guiding the analysis and justifies the chosen modeling techniques. Additionally, it provides a structured methodology to ensure consistency, accuracy, and reproducibility of the results.

2.1 The Skyrme Interaction

In 1958, Skyrme introduced the Skyrme interaction, a phenomenological zero-range force that has been extensively employed within the Hartree-Fock (HF) mean-field framework, which is a self-consistent approach [18]. This interaction replaces the realistic nucleon-nucleon force with a contact potential that effectively simulates the short-range nature of the nuclear force while

maintaining computational efficiency [19]. The Skyrme force consists of a zero-range three- body term and two momentum-dependent two- body terms. Within the Hartree-Fock formalism, the density-dependent three-body term can be effectively replaced by an equivalent two-body interaction. Consequently, the Skyrme interaction can be expressed in a compact and unified form known as the extended Skyrme force [20].

The general expression of the Skyrme interaction is given by:

$$v_{12} = t_0\left(1 + x_0\hat{P}_\sigma\right)\delta(\vec{r}_1 - \vec{r}_2) + \frac{t_1}{2}\left(1 + x_1\hat{P}_\sigma\right)$$
$$\left(\hat{k}^2\delta(\vec{r}_1 - \vec{r}_2) + \delta(\vec{r}_1 - \vec{r}_2)\hat{\acute{k}}^2\right) + t_2\left(1 + x_2\hat{P}_\sigma\right)\hat{\acute{k}}.\delta(\vec{r}_1 - \vec{r}_2)\hat{k}$$
$$+\frac{t_3}{6}\left(1 + x_3\hat{P}_\sigma\right)\rho^\alpha\left(\vec{R}\right)\delta(\vec{r}_1 - \vec{r}_2) + iW_0\hat{\acute{k}}(\hat{\sigma}_1 + \hat{\sigma}_2) \times \hat{k}\delta(\vec{r}_1 - \vec{r}_2) \quad (1)$$

Here, $\vec{\boldsymbol{R}} = \frac{\vec{\boldsymbol{r}}_1 + \vec{\boldsymbol{r}}_2}{\boldsymbol{2}}$, and the Skyrme interaction parameter is denoted by $\boldsymbol{\alpha}$. The operators

$$\hat{\boldsymbol{k}} = \left(\vec{\boldsymbol{\nabla}}_1 - \vec{\boldsymbol{\nabla}}_2\right)/2\boldsymbol{i} \text{ and } \hat{\acute{\boldsymbol{k}}} = -\left(\acute{\vec{\boldsymbol{\nabla}}}_1 - \acute{\vec{\boldsymbol{\nabla}}}_2\right)/2\boldsymbol{i} \quad (2)$$

denote the relative momentum operators acting on the wave functions to the right and left, in that order. free parameters $\boldsymbol{t_0, t_1, t_2, t_3, x_1, x_2, x_3}$ and $\boldsymbol{W_0}$ are used to calibrate experimental nuclear structure data and describe the intensities of the various interaction components.

The Pauli matrices $\hat{\boldsymbol{\sigma}}$, the spin-exchange operator $\hat{\boldsymbol{P}}_{\boldsymbol{\sigma}} = \frac{\boldsymbol{1}}{\boldsymbol{2}}\left(\boldsymbol{1} + \hat{\boldsymbol{\sigma}}_{\boldsymbol{1}} \cdot \hat{\boldsymbol{\sigma}}_{\boldsymbol{2}}\right)$, and the Dirac delta function $\boldsymbol{\delta}(\vec{\boldsymbol{r}}_{\boldsymbol{1}} - \vec{\boldsymbol{r}}_{\boldsymbol{2}})$ are used in the formulation of the interaction.

2.2 Skyrme Interaction (Sk29)

In the present work, the Sk29 parameterization is employed to generate single-particle radial wave functions. It is important to note that the Skyrme interaction is not employed within a fully self-consistent Hartree-Fock calculation. Instead, it is used to generate single-particle radial wave functions that serve as input for the shell-model calculations. The detailed parameter set of Sk29 is taken from the literature and is summarized in **Table 1** for completeness and reproducibility. These parameters define the strength of the central, spin-orbit, and density-dependent terms of the effective interaction. These parameters provide a reliable description of medium-mass nuclear properties.

Table 1: Skyrme (Sk29) parameter set used in this work

Parameter	Value
t_0 (MeV fm^3)	-2488.91
t_1 (MeV fm^5)	486.82
t_2 (MeV fm^5)	-546.39
t_3 (MeV fm$^{3+3\alpha}$)	13777.0
x_0	0.834
x_1	-0.344
x_2	-1.000
x_3	1.354
A	1/6
W_0 (MeV fm^5)	123.0

These parameters are widely used in mean-field calculations and provide a reliable description of medium-mass nuclear properties.

2.3 Woods-Saxon Potential (WS3)

An often-used tool for describing the mobility of individual nucleons in nuclei is the Woods-Saxon (WS) potential. As a one- body potential, it neglects explicit two-body interactions and therefore cannot determine the total binding energy[21]. Solving the radial equation yields the single-particle wave functions.

$$\left[-\frac{\hbar^2}{2\mu}\frac{d^2}{dr^2} + \frac{\hbar^2 l(l+1)}{2\mu r^2} + U(r)\right] R(j,r) = \varepsilon\, R(j,r) \qquad (3)$$

where the total potential $U(r)$consists of a central Woods-Saxon term, a spin-orbit interaction, and a Coulomb potential for protons. The radius is parameterized as $R = r_0 A^{\frac{1}{3}}$

The Woods–Saxon potential is commonly expressed as:

$$V(r) = -\frac{V_0}{1+\exp\left(\frac{r-R}{a}\right)} \qquad (4)$$

In the present work, the WS3 parameterization is employed to generate single-particle radial wave functions. The parameters used in this work are summarized in **Table 2**.

Table 2: Woods–Saxon (WS3) parameters used in this work

Parameter	Value
Central depth V_o	50 MeV
Radius parameter r_o	1.25 fm
Diffuseness a	0.65 fm
Spin–orbit strength V_{so}	6 MeV

These parameters provide a realistic description of the nuclear surface and spin–orbit splitting.

2.4 Harmonic Oscillator Potential (HT)

The harmonic oscillator (HT) potential is widely used as a simple model for descripting single-particle motion in nuclei. It provides an approximate description of the nuclear mean field, particularly for light nuclei. In this model, nucleons are treated as independent particles moving in a spherically symmetric potential. The corresponding Hamiltonian is given by [21]:

$$H_o = \frac{-\hbar^2}{2m}\nabla^2 + \frac{m\omega^2 r^2}{2} - U_o \quad (5)$$

The Schrödinger equation yields eigenstates that separate into radial and angular parts, expressed in terms of harmonic oscillator radial wave functions and spherical harmonics. To account for the observed magic numbers, a strong spin–orbit interaction is included, which splits each orbital into $j = l \pm \frac{1}{2}$ levels within the jj-coupling scheme. It is generally believed that the spin-orbit term's strength scales as $A^{-\frac{2}{3}}$. Single-particle states are therefore specified by the quantum numbers n, l, j and isospin, which distinguishes protons from neutrons [22].

In the present work, the harmonic oscillator (HT) is used as a reference model due to its analytical simplicity, although it lacks realistic surface behavior compared to more sophisticated potentials such as Woods-Saxon.

3. Results and Discussion.

The results are analyzed with particular emphasis on the sensitivity of the calculated form factors to the choice of radial wave functions. This section provides a comprehensive analysis of the calculated results, with a focus on their physical interpretation and comparison with available experimental data for sd-shell nuclei. The shell-model calculations are performed using the NuShellX@MSU code within

the proton-neutron formalism [17]. In the present work, the Sk29 interaction is employed in conjunction with Woods-Saxon (WS) and harmonic oscillator (HT) radial wave functions within the sd-shell model space, consistent with previous studies demonstrating the effectiveness of Skyrme-type interactions in describing nuclear structure properties . These ingredients are used to construct the effective two-body matrix elements and to investigate their impact on charge distributions and inelastic electron-scattering form factors. For clarity, the discussion is organized into two main parts. The first part presents the inelastic electron-scattering form factors, excitation energies, and transition probabilities for positive-parity states, ordered according to increasing angular momentum. This is followed by a detailed analysis of the corresponding negative-parity states. Throughout this section, the numerical results are complemented by a physical interpretation and a systematic comparison with experimental data, highlighting both the predictive capability and the limitations of the adopted shell-model framework.

3.1 Positive parity states

The longitudinal (Coulomb) and transverse electron-scattering form factors of selected low- lying positive-parity states in ^{19}F are investigated within the sd-shell model space using the Sk29 interaction together with Woods-Saxon (WS3) and harmonic oscillator (HT) radial wave functions. The calculated results are compared with available experimental data over a wide range of momentum transfer. At low momentum transfer, all three potentials reproduce the experimental data well, indicating that the long-range behavior of the wave functions is properly described. However, at higher momentum transfer, noticeable differences emerge, reflecting the sensitivity of the form factors to the radial structure. The HT potential underestimates the high-momentum components due to its Gaussian behavior, whereas Sk29 and WS3 provide improved agreement owing to their more realistic asymptotic properties.

Fig. $1 - E_x = 0.00\text{MeV}, J^\pi = 1/2^+$ The calculated Coulomb monopole C0 form factors obtained with Sk29, WS3, and HT reproduce the experimental trend very well in the low-q region and correctly capture the characteristic diffraction pattern. A pronounced minimum is predicted at $q \approx 1.6\ \text{fm}^{-1}$,followed by a weaker second lobe at higher momentum transfer. Beyond the minimum, modest interaction-

dependent differences appear, reflecting the increasing sensitivity of the C0 response to the high-q components of the radial charge density and short-range aspects of the single-particle wave functions.

For the transverse M1 form factor, the calculations reproduce the overall two-lobe behavior and describe the low-q strength reasonably well. However, the theoretical curves predict a deeper minimum than indicated by the data in the intermediate-q region and tend to underestimate the strength around and beyond the minimum. This pattern is consistent with the enhanced sensitivity of transverse magnetic transitions to operator renormalization effects-most notably core polarization and possible two-body current contributions-which become increasingly important at intermediate and high momentum transfer.

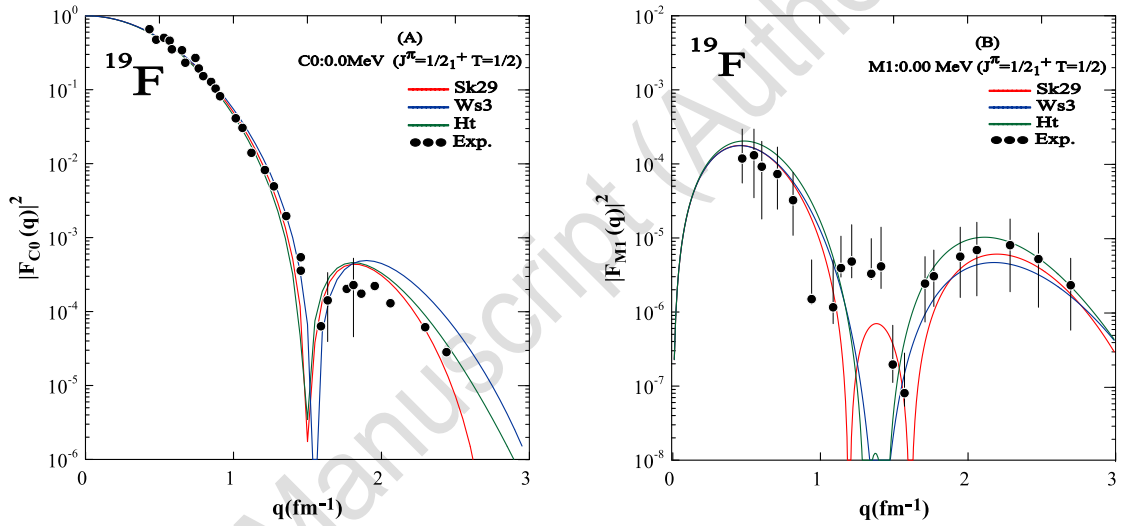

Fig. 1. Calculated longitudinal (A) and transverse (B) form factors for the $J^\pi = 1/2^+$ state, compared with experimental data from Ref. [3].

Fig.2 $-E_x = 1.554$ MeV, $J^\pi = 3/2^+$ The calculated C2 longitudinal form factors obtained with Sk29, WS3, and HT display a highly consistent description of the data in the low- and intermediate-q region. All interactions reproduce the first lobe, with the main maximum located at $q \approx 0.8 - 1.0\ \mathrm{fm}^{-1}$, and generate a pronounced diffraction minimum around $q \approx 1.8 - 1.9\ \mathrm{fm}^{-1}$. The agreement in both the magnitude and the location of these characteristic features indicates that the transition charge density and the associated quadrupole collectivity for this excitation are reliably captured within the adopted sd-shell framework. The small residual differences among the interactions become noticeable mainly beyond the

minimum and at higher momentum transfers, where the form factor is more sensitive to the radial tails of the wave functions and to missing short-range correlations and higher-order configurations outside the restricted model space.

For the transverse (M1 + E2) response, the three calculations follow the global experimental behavior through the first maximum ($q \sim 0.9\ \mathrm{fm}^{-1}$)and correctly predict the diffraction minimum near $q \approx 1.55 - 1.65\ \mathrm{fm}^{-1}$. The magnitude in the low-q region is reasonably reproduced, supporting an adequate balance between the orbital and spin contributions in the electromagnetic transition operator. At larger momentum transfers, the theoretical curves exhibit an increasing spread and tend to underestimate the second-lobe strength relative to the data, reflecting the enhanced sensitivity of the transverse channel to interaction details and to missing renormalization effects, such as core polarization and possible two-body current contributions, which become increasingly important at higher q.

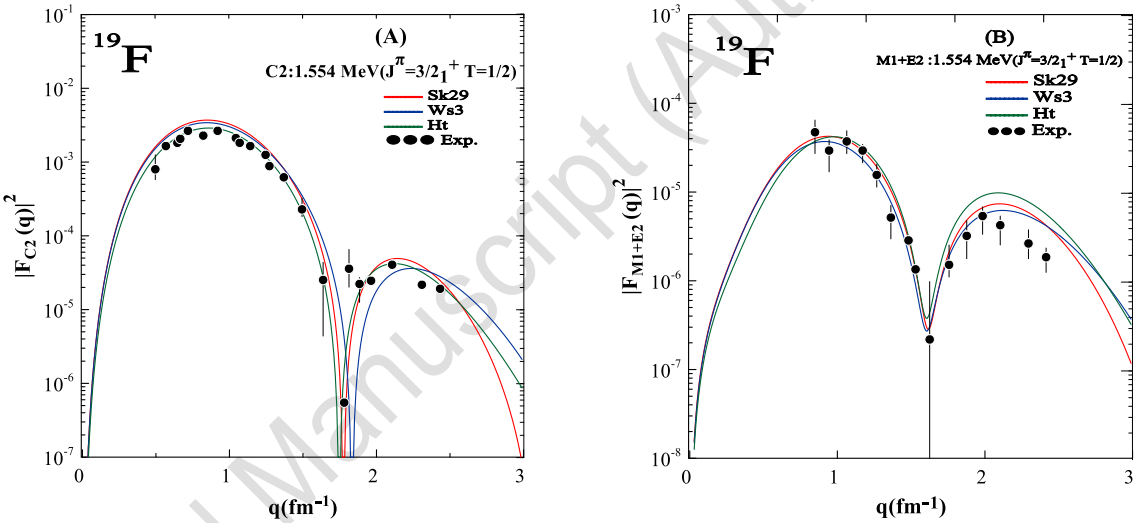

Fig. 2. Calculated longitudinal (A) and transverse (B) form factors for the $J^{\pi} = 3/2^{+}$+ state, compared with experimental data from Ref. [3].

Fig. $3 - E_x = 0.197\ \mathrm{MeV}, J^{\pi} = 5/2^{+}$ The calculated C2 form factors reproduce the experimental trend well in the low-momentum- transfer region and provide a consistent prediction for the position of the diffraction minimum. The close grouping of the Sk29, WS3, and HT results indicates that the transition charge density for this excitation is rather robust within the adopted sd -shell description, with only moderate interaction dependence emerging as q increases.

For the transverse E2 + M3 response, the three calculations reproduce the overall behavior of the experimental form factor up to intermediate momentum transfer. At

higher q values, systematic deviations emerge, indicating an increased sensitivity to (i) configuration mixing beyond the sd-shell model space and (ii) renormalization effects in the transverse transition operators. In this momentum-transfer region, contributions arising from core polarization and two-body current mechanisms are expected to play a progressively more significant role.

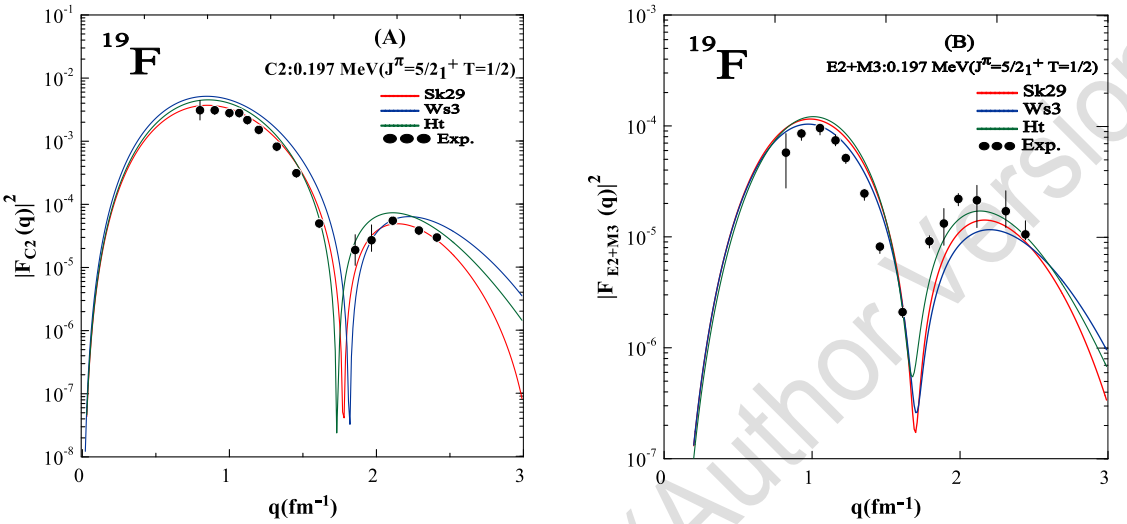

Fig. 3. Calculated longitudinal (A) and transverse (B) form factor for the $J^{\pi} = 5/2^{+}$ state, compared with experimental data from Ref. [3].

Fig. 4 $-E_x = 4.378\text{MeV}, J^{\pi} = 7/2^{+}$ The C4 longitudinal form factor for this higher-spin excitation is characterized by comparatively weak strength and limited experimental coverage. Despite the sparsity of the data, the calculations capture the overall magnitude and the broad q -dependence reasonably well, indicating that the dominant features of the underlying transition charge density are described satisfactorily within the present framework.

In the transverse channel, the predicted form factors agree with the measured trend at low q, while differences among interactions become more apparent at intermediate momentum transfers. In particular, the HT interaction yields slightly enhanced strength relative to Sk29 and WS3 in parts of the q-range, reflecting the increased sensitivity of higher-multipole transverse transitions to the radial structure of the wave functions and to interaction-dependent spin-orbit and tensor-like components effectively encoded in the employed mean-field parametrizations.

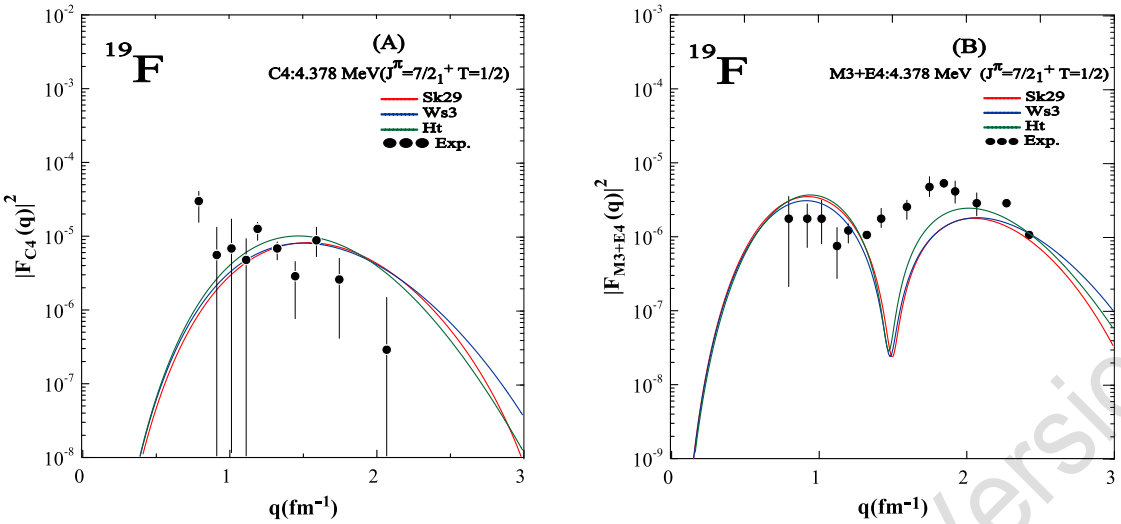

Fig. 4. Calculated longitudinal (A) and transverse (B) form factors for the $J^\pi = 7/2^+$ state, compared with experimental data from Ref. [3].

Fig. $5 - E_x = 2.779$ MeV, $J^\pi = 9/2^+$ As illustrated in panel (A), the calculated longitudinal C4 form factors show excellent agreement with the experimental data. The three interactions (Sk29, WS3, and HT) successfully reproduce the overall profile and correctly position the principal maximum near $q \approx 1.4\ \mathrm{fm}^{-1}$. The strong overlap of the theoretical curves over most of the measured momentum-transfer range reflects a robust and well-constrained description of the longitudinal C4 component within the adopted model space.

In contrast, the calculated E4 + M5 transverse form factors systematically underestimate the experimental strengths over a broad momentum- transfer range, although the predicted shape and approximate position of the maximum are qualitatively reasonable. This shortfall is consistent with the known limitations of a restricted sd-shell description for high-multipolarity transverse transitions, where missing contributions from core polarization, higher-shell admixtures, and two- body (meson-exchange) currents can be non- negligible. Incorporating extended configuration spaces and/or employing effective (renormalized) transverse operators is therefore expected to improve the agreement for this transition.

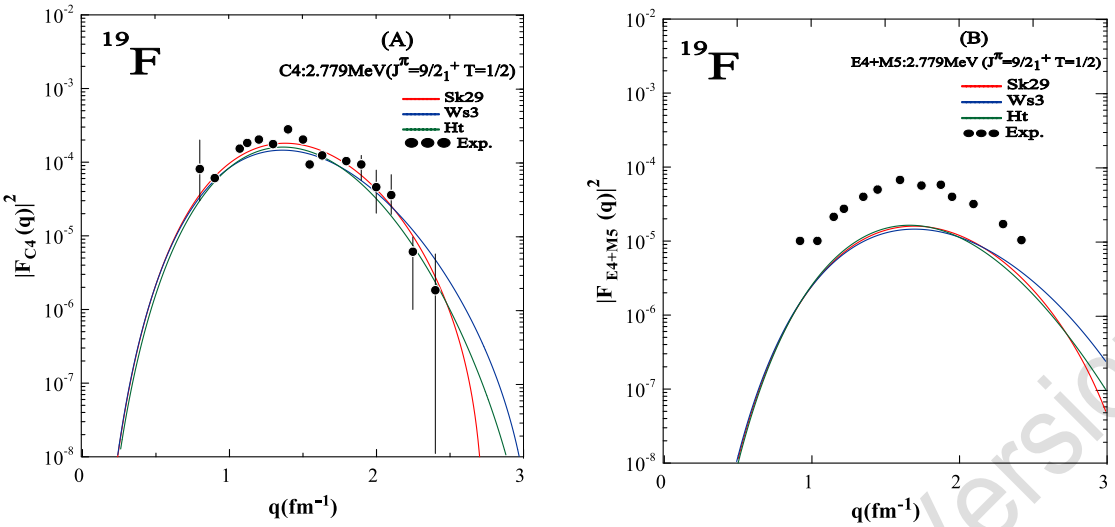

Fig. 5. Calculated longitudinal (A) and transverse (B) form factors for the $J^{\pi} = 9/2^{+}$ state, compared with experimental data from Ref. [3].

3.2 Negative parity states

The longitudinal and transverse electron-scattering form factors for selected negative-parity states in ^{19}F are calculated using the Sk29 interaction together with Woods-Saxon (WS3) and harmonic oscillator (HT) radial wave functions and compared with available experimental data over a range of momentum transfer. The results indicate that negative-parity states exhibit a stronger sensitivity to the radial structure, particularly in the longitudinal channel. At intermediate momentum transfer, noticeable discrepancies are observed, suggesting that additional correlations beyond the restricted sd-shell model space may be required. The transverse responses reproduce the overall shape of the experimental data more reliably however, deviations in magnitude persist, indicating the need for improved effective operators, including core polarization and two- body current contributions. Fig.6 $-\ E_x = 0.1098\text{MeV}, J^{\pi} = 1/2^{-}$ The longitudinal Coulomb form factor $|F_{C1}(q)|^2$, shown in panel (A), exhibits a pronounced maximum at low momentum transfer followed by a rapid decrease and a deep minimum around $q \approx 1.5\ \text{fm}^{-1}$, characteristic of diffraction effects arising from the finite spatial extension of the transition density. All three theoretical interactions forecast a comparable qualitative trend; however, significant inconsistencies with the experimental results emerge in the region $q \approx 0.8 - 1.3\ \text{fm}^{-1}$, where the computed transition strengths fall short of the observed values. This trend shows that the C1 transition is quite sensitive to the precise radial structure of

the wave functions. The transverse electric response $|F_{E1}(q)|^2$,, shown in panel (B), has a wide bell-shaped distribution with a peak around $q \approx 1.5\ \mathrm{fm}^{-1}$. The theoretical results better match the size and overall form of the experimental data than the longitudinal component. This suggests that the transverse response is less affected by short-range correlations that depend on the model.

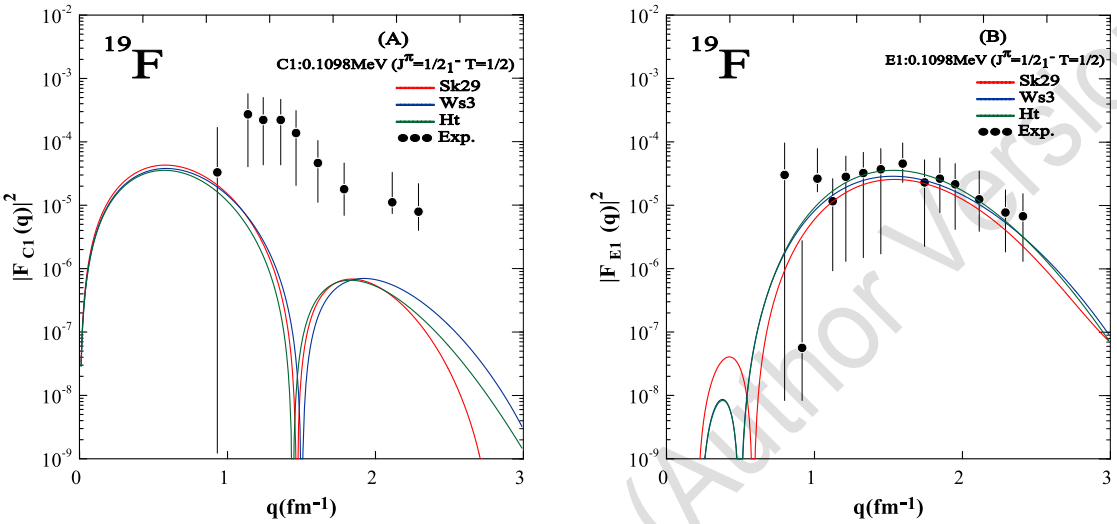

Fig. 6. Computed longitudinal (A) and transverse (B) form factors for the $J^{\pi} = 1/2^{-}$state; experimental data are from Ref. [3].

Fig. $7 - E_x = 1.459\ \mathrm{MeV}, J^{\pi} = 3/2^{-}$ The computed C1 form factor displays a prominent low-q peak, succeeded by a significant minimum at approximately $q \approx 1.6\ \mathrm{fm}^{-1}$and a secondary maximum at elevated momentum transfer. The experimental data show that the intermediate area $q \approx 0.7 - 1.2\ \mathrm{fm}^{-1}$ is stronger than all three interactions predicted. This shows that the modeled charge transition density for this state is not very good. The transverse response, which includes both electric dipole (E1) and magnetic quadrupole (M2) contributions, has a typical interference pattern with a deep minimum around $q \approx 1.9\ \mathrm{fm}^{-1}$. The theoretical models do a good job of showing where this minimum is, but the varying depths show how the electric and magnetic balances are different in each interaction.

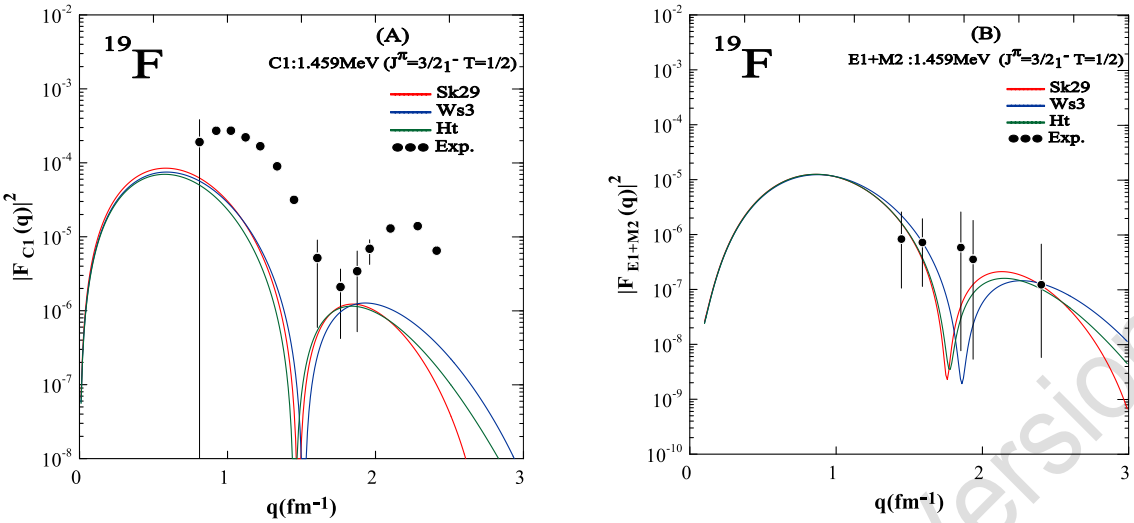

Fig. 7. Computed longitudinal (A) and transverse (B) form factors for the $J^{\pi} = 3/2^{-}$ state; experimental data are from Ref. [3].

Fig. $8 - E_x = 1.34567$ **MeV**, $J^{\pi} = 5/2^{-}$ The Coulomb octupole form factor $|F_{C3}(q)|^2$, seen in panel (A), rises steadily to a peak at $q \approx 1.2\ \mathrm{fm}^{-1}$ and subsequently declines smoothly at elevated momentum transfer. The strong correlation between the three theoretical curves and the experimental data suggests that the significant characteristics of the transition density are well represented for this negative-parity state. The transverse response, which includes contributions from magnetic quadrupole and electric octupole, as depicted in panel (B), demonstrates significant model dependence. While all interactions reflect the overall trend of the data, significant variations in magnitude persist, highlighting the susceptibility of higher-multipole transverse transitions to the fundamental nuclear structure and configuration mixing.

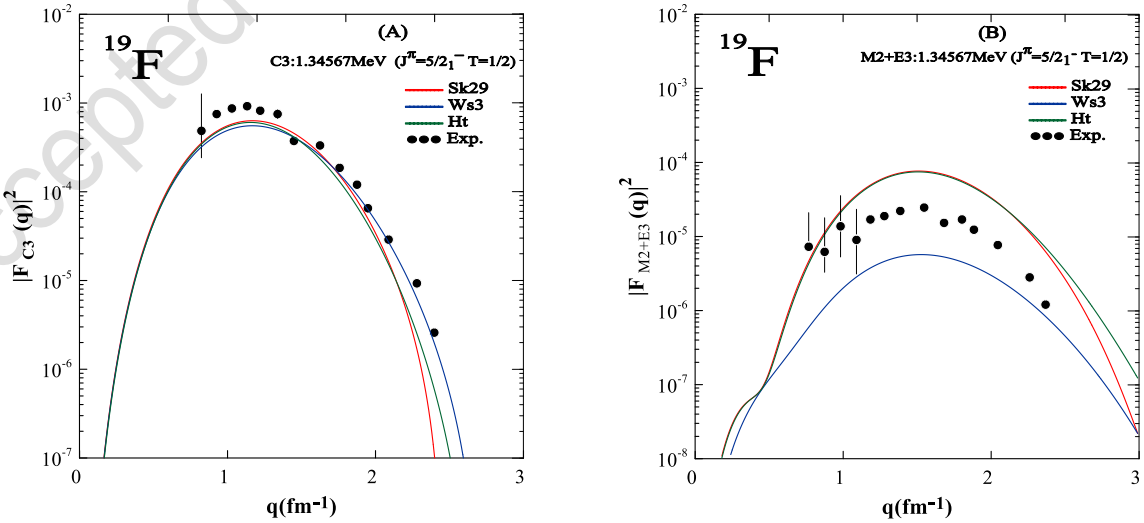

Fig. 8. Computed longitudinal (A) and transverse (B) form factors for the $J^{\pi} = 5/2^{-}$ state; experimental data are from Ref. [3].

Fig. 9 – $E_x = 3.9987$ MeV, $J^\pi = 7/2^-$ The Coulomb octupole form factor $|F_{C3}(q)|^2$, which is depicted in panel (A). The computed response has a distinct maximum, accompanied by a slow decline. In general, the results follow the experimental trend within the given uncertainties, but there are some small differences for larger momentum transfer. These disparities may indicate the inadequate representation of high-momentum components within the selected model space. The total transverse response, which includes the E3 and M4 multipole contributions and is shown in panel (B), has clear diffraction patterns with clear minima near $q \approx 1.0\ \mathrm{fm}^{-1}$ and $q \approx 2.7\ \mathrm{fm}^{-1}$ .The theoretical curves accurately depict the positions of these minima; nevertheless, discrepancies in their depth indicate the substantial sensitivity of higher-order multipole transitions to the intricate current distributions and spin-orbit structure inherent in nuclear wave functions.

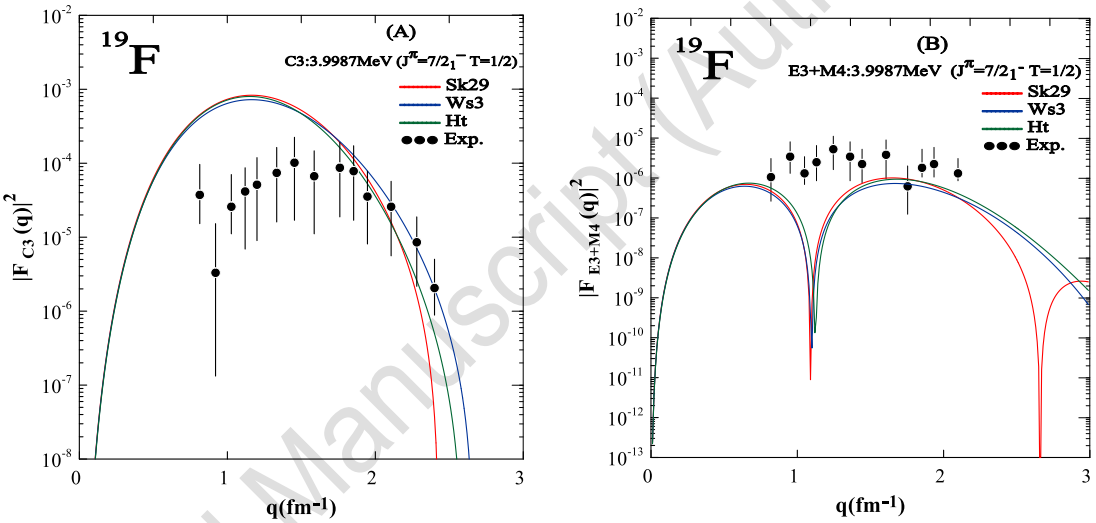

Fig. 9. Computed longitudinal (A) and transverse (B) form factors for the $J^\pi = 7/2^-$ state; experimental data are from Ref. [3].

4.Conclusions

The sd-shell calculations using the Skyrme- type effective interactions Sk29, WS3, and HT provide a consistent and reliable description of the inelastic electron-scattering systematics in ^{19}F. For low-lying positive-parity states, the longitudinal (Coulomb) form factors are reproduced with high accuracy at low and intermediate momentum transfers. In particular, the positions of diffraction maxima and minima are consistently captured, demonstrating that the corresponding transition charge densities are structurally reliable within the adopted model space. The transverse response is also well reproduced in the low-q regime; however, the emergence of increasing deviations at higher q and for higher multipolarities exposes the limits of the present operator/space truncation, where neglected renormalization effects become non-negligible. For negative-parity excitations, the longitudinal channel becomes a more discriminating probe of the underlying radial structure and configuration mixing, leading to systematic mismatches in the intermediate-q region that cannot be removed by interaction changes alone.

By contrast, the transverse electric and magnetic form factors retain the correct global morphology-including peak ordering and overall momentum-transfer dependence-across the three interactions. Nevertheless, systematic discrepancies remain in the absolute strengths and in the depth of diffraction minima, particularly for higher multipolarities. Taken together, these residual differences-most evident at large q and in the transverse channel- provide compelling evidence that correlations beyond the restricted sd-shell space, together with improved effective electromagnetic operators, are required. In particular, explicit core-polarization renormalization and, where relevant, two-body current contributions appear essential for a quantitatively consistent description.

A systematic and controlled comparison of different radial wave functions has been performed for ^{19}F. The results clearly demonstrate that the choice of radial wave functions plays a crucial role in determining electron-scattering form factors. In particular, the Sk29 and WS3 potentials provide improved agreement with experimental data compared to the harmonic oscillator potential, especially at higher momentum transfer. The remaining discrepancies highlight the need for extended model spaces and improved effective operators.

Declarations

Sources of Funds

No fund or grant was received for conducting this study.

Competing Interests

The authors declare that they have no competing interests.

Author's Contribution

Ali Abdulmajeed Mohsin: Conceptualization, Methodology, Software, Investigation, Data curation, Formal analysis, Writing-original draft, Writing-review & editing.

Fouad A. Majeed: Supervision, Validation, Resources, Writing-review & editing.

Data Availability Statement

The data that support the findings of this study are available from the corresponding author upon reasonable request.

References

[1] Hallowell PL, Bertozzi W, Heisenberg J, Kowalski S, Maruyama X, Sargent CP, Turchinetz W, Williamson CF, Fivozinsky SP, Lightbody Jr JW, Penner S. Electron Scattering from ^{19}F and ^{40}Ca. Physical Review C. 1973 Apr 1;7(4):1396.
https://doi.org/10.1103/PhysRevC.7.1396

[2] Oyamada M, Terasawa T, Nakahara K, Endo Y, Saito H, Tanaka E. Electroexcitation of low-lying states in ^{19}F. Physical Review C. 1975 May 1;11(5):1578.
https://doi.org/10.1103/PhysRevC.11.1578

[3] Brown BA, Wildenthal BH, Williamson CF, Rad FN, Kowalski S, Crannell H, O'brien JT. Shell-model analysis of high-resolution data for elastic and inelastic electron scattering on ^{19}F. Physical Review C. 1985 Oct 1;32(4):1127.
https://doi.org/10.1103/PhysRevC.32.1127

[4] Williamson CF, Rad FN, Kowalski S, Heisenberg J, Crannell H, O'Brien JT, Lee HC. Electroexcitation of the Ground-State Rotational Band in F 19. Physical Review Letters. 1978 Jun 26;40(26):1702.
https://doi.org/10.1103/PhysRevLett.40.1702

[5] Sakuda T. Cluster Model Study of Electron Scattering on ^{19}F. Progress of Theoretical Physics. 1992 May 1;87(5):1159-69.
https://doi.org/10.1143/ptp/87.5.1159

[6] Radhi RA, Abdullah AA, Raheem AH. Calculations of elastic and inelastic electron scattering on 19F using large-basis no core-shell model wave functions. Nuclear Physics A. 2008 Jan 1;798(1-2):16-28.
https://doi.org/10.1016/j.nuclphysa.2007.10.010

[7] Majeed FA, Obaid SM. Nuclear structure study of ^{22,24}Ne and ^{24}Mg nuclei. Revista mexicana de física. 2019 Apr;65(2):159-67.
https://doi.org/10.31349/revmexfis.65.159

[8] Obaid SM, Majeed FA. Longitudinal and transverse form factors from ^{65}Cu and ^{71}Ga nuclei. Journal of the Korean Physical Society. 2023 Feb;82(4):329-39.
https://doi.org/10.1007/s40042-022-00682-w

[9] Obaid SM, Abbas SA, Hussein AA, Mohammed NA, Majeed FA. Shell Model Investigation of Some p and sd-Shell Nuclei with Harmonic Oscillator and Skyrme Interactions. East European Journal of Physics. 2023 Jun 2(2):91-7.
https://doi.org/10.26565/2312-4334-2023-2-07

[10] AbdulRidha AH, Majeed FA, Hussain FM. Electron scattering form factors of ^{24}Mg, ^{28}Si and ^{32}S: a shell model study with core polarisation. International Journal of Nuclear Energy Science and Technology. 2025;18(1):41-57.
https://doi.org/10.1504/IJNEST.2025.148439

[11] Talib TM, Majeed FA. Study of the nuclear structure for ^{7}Li, ^{9}Be and ^{24}Mg with Skyrme effective interaction. International Journal of Nuclear Energy Science and Technology. 2024;17(2-3):165-79.
https://doi.org/10.1504/IJNEST.2024.142756

[12] Alzubadi AA. Investigating the Impact of the Nuclear Single- Particle Potentials on Parity-Changing Transitions and Deformation in 24Mg. Journal of Theoretical and Applied Physics. 2025 Dec 31;19(6).
https://doi.org/10.57647/j.jtap.2025.1906.53

[13] Mohammed SB, Latif NT, Talib TM, Sameer AS, Obaid SM, Majeed FA. Systematic Shell-Model Evaluation of Gamow-Teller Transitions in ^{13}C, ^{13}N, ^{13}O, ^{23}Na and ^{23}Na Nuclei: Validation of Effective Interactions and Quenching Effects. High Energy Density Physics. 2025 Nov 8:101240.
https://doi.org/10.1016/j.hedp.2025.101240

[14] Talib TM, Majeed FA. Study of the nuclear structure of some FP-shell nuclei with Skyrme effective interaction. Nuclear Physics A. 2025 Apr 1;1056:123021.
https://doi.org/10.1016/j.nuclphysa.2025.123021

[15] Chambers-Wall G, Gnech A, King GB, Pastore S, Piarulli M, Schiavilla R, Wiringa RB. Quantum Monte Carlo calculations of magnetic form factors in light nuclei. Physical Review Letters. 2024 Nov 22;133(21):212501.
https://doi.org/10.1103/PhysRevLett.133.212501

[16] Miyagi T, Heinz M, Schwenk A. Ab initio computations of the fourth-order charge density moments of ^{48}Ca and ^{208}Pb. Physics Letters B. 2025 Nov 17:140032. https://doi.org/10.1016/j.physletb.2025.140032
[17] Brown BA, Rae WD. The shell-model code NuShellX@ MSU. Nuclear Data Sheets. 2014 Jun 1;120:115-8. https://doi.org/10.1016/j.nds.2014.07.022
[18] Skyrme TH. The effective nuclear potential. Nuclear Physics. 1958 Jan 1;9(4):615-34. https://doi.org/10.1016/0029-5582(58)90345-6
[19] Vautherin D, Brink DM. Hartree-Fock calculations with Skyrme's interaction. Physics Letters B. 1970 Jun 22;32(3):149-53. https://doi.org/10.1016/0370-2693(70)90458-2
[20] Sarriguren P, Moreno O, Moya de Guerra E, Kadrev DN, Antonov AN, Gaidarov MK. Elastic Magnetic Electron Scattering from odd-A Nuclei. InJournal of Physics: Conference Series 2020 May 1 (Vol. 1555, No. 1, p. 012001). IOP Publishing. https://doi.org/10.1088/1742-6596/1555/1/012001
[21] Walecka JD. Theoretical nuclear and subnuclear physics. World Scientific Publishing Company; 2004 Sep 29. https://doi.org/10.1142/5500
[22] de la Ripelle MF, Sofianos SA, Adam RM. Method for solving the many-body bound state nuclear problem. Annals of Physics. 2005 Mar 1;316(1):107-59. https://doi.org/10.1016/j.aop.2004.09.006